

RESEARCH

Open Access



# Exosomes containing circSCP2 in colorectal cancer promote metastasis via sponging miR-92a-1-5p and interacting with PTBP1 to stabilize IGF2BP1

Qing Meng<sup>1,2†</sup>, Haoyi Xiang<sup>1,2†</sup>, Yijing Wang<sup>1,2†</sup>, Kepeng Hu<sup>1,2†</sup>, Xin Luo<sup>1,4</sup>, Jiawei Wang<sup>1,2</sup>, Engeng Chen<sup>1,2</sup>, Wei Zhang<sup>1,2</sup>, Jiaxin Chen<sup>1,5</sup>, Xiaoyu Chen<sup>1,2</sup>, Huogang Wang<sup>1,2</sup>, Zhenyu Ju<sup>3</sup> and Zhangfa Song<sup>1,2\*</sup>

## Abstract

Exosomes have emerged as significant biomarkers for multiple diseases, including cancers. Circular RNAs (circRNAs), abundant in exosomes, are involved in regulating cancer development. However, the regulatory function and the underlying molecular mechanism of hsa\_circ\_0006906 (circSCP2) in colorectal cancer (CRC) metastasis remain unclear. A competing endogenous RNA microarray was used to analyze circRNA expression in serum exosomes in patients with CRC at early and late stages. circSCP2 expression was evaluated using qRT-PCR. The biological functions of circSCP2 in CRC were assessed through in vitro and in vivo experiments. The molecular mechanism of circSCP2 was explored using western blotting, RNA pulldown, RNA immunoprecipitation, luciferase assays, and relative rescue experiments. circSCP2 expression was significantly elevated in CRC tissues, with higher levels in serum exosomes correlating with advanced TNM stages. circSCP2 knockdown inhibited CRC cell proliferation, migration, invasion, and metastasis in vitro and in vivo. Mechanistically, circSCP2 sponged miR-92a-1-5p to increase insulin-like growth factor 2 mRNA-binding protein 1 (IGF2BP1) expression. Additionally, circSCP2 directly bound to and stabilized polypyrimidine tract binding protein 1 (PTBP1) by inhibiting protein ubiquitination, resulting in IGF2BP1 mRNA stabilization and enhanced CRC migration and invasion. Our findings demonstrate that circSCP2 regulates the miR-92a-1-5p/IGF2BP1 pathway, promotes PTBP1/IGF2BP1 interaction, and accelerates CRC progression. Exosomal circSCP2 is a promising circulating biomarker for CRC prognosis and needs further therapeutic investigation.

**Keywords** circRNA, Colorectal cancer, IGF2BP1

<sup>†</sup>Qing Meng, Haoyi Xiang, Yijing Wang, and Kepeng Hu contributed equally to this work.

\*Correspondence:

Zhangfa Song  
songzhangfa@zju.edu.cn

<sup>1</sup>Department of Colorectal Surgery, Sir Run Run Shaw Hospital, Zhejiang University School of Medicine, Hangzhou 310016, China

<sup>2</sup>Key Laboratory of Biological Treatment of Zhejiang Province, Hangzhou 310016, China

<sup>3</sup>Key Laboratory of Regenerative Medicine of Ministry of Education, Institute of Aging and Regenerative Medicine, Jinan University, Guangzhou 510632, China

<sup>4</sup>Present address: Department of Thyroid and Breast Surgery, Taizhou Enze Medical Center (Group), Enze Hospital, Taizhou 318000, China

<sup>5</sup>Present address: Department of Breast Surgery, The Second Affiliated Hospital, Zhejiang University School of Medicine, Hangzhou 310009, China



## Background

Colorectal cancer (CRC) is the third most common malignant tumor worldwide and the second leading cause of cancer-related death [1]. While primary CRC can be surgically treated, the average 5-year overall survival rate in China remains at 60%, even after surgery. Approximately 20% of patients present with synchronous liver metastases (LM) at diagnosis. Metastasis is the leading cause of death, highlighting the need for additional therapeutic targets to prevent metastasis and increase the overall survival of metastatic CRC.

Circular RNAs (circRNAs) are non-coding RNAs that have attracted significant attention. Unlike linear RNA, its 3' and 5' terminals are connected by reverse splicing, making them resistant to degradation by exonuclease RNase R and thus more stable [2–4]. Evidence suggests that circRNAs play vital roles in regulating carcinogenesis and cancer progression, often by binding microRNAs (miRNAs) and regulating downstream target gene expression at the post-transcriptional level [4–6]. Recent studies also confirmed that circRNAs can interact with RNA-binding proteins (RBPs) to modulate their interacted mRNA stability and function [4–8]. However, the mechanisms of circRNAs in CRC remain poorly understood. Cancer-derived exosomes are small vesicles (30–100 nm in diameter) that travel through interstitial spaces and body fluids such as blood and urine [4, 9, 10]. These exosomes, enriched with circRNAs, can be transported to receptor cells, modulating tumor invasion, angiogenesis, immune escape, and metastasis [4, 11]. For example, Li et al. revealed that pancreatic cancer cells could secrete exosomal circIARS to increase vascular permeability, promoting tumor invasion and metastasis. Similarly, Wang et al. discovered that oxaliplatin-resistant CRC cells secreted and delivered exosomal hsa\_circ\_0005963 to sensitive cells to promote glycolysis and drug resistance through the miR-122-PKM2 axis [12]. Exosomes thus play important roles as cargoes between tumor cells and microenvironments. Recent studies have focused on circRNAs in exosomes to improve accuracy in tumor diagnosis and treatment.

This study revealed that hsa\_circ\_0006906 (circSCP2) was significantly upregulated in plasma exosomes from patients with CRC and metastases compared with those from early-stage patients. Additionally, circSCP2 was highly expressed in CRC tissues and positively correlated with advanced tumor progression. CRC cells with elevated circSCP2 expression exhibited a strong ability for growth, migration, and epithelial-to-mesenchymal transition (EMT) *in vitro* and *in vivo*. Further exploration indicated that circSCP2 can restore cancer-promoting insulin-like growth factor 2 mRNA-binding protein 1 (IGF2BP1) expression via sponging miR-92a-1-5p, ultimately promoting CRC metastasis. Additionally, we also

discovered that circSCP2 interacted with Polypyrimidine Tract Binding Protein 1 (PTBP1), inhibiting ubiquitylation-induced PTBP1 degradation, hence enhancing IGF2BP1 mRNA stabilization.

Moreover, CRC cells with elevated circSCP2 expression exhibited reduced sensitivity to Oxaliplatin. And surprisingly, we confirmed exosomal circSCP2 uptake could activate carcinoma-associated fibroblast (CAF) precursor LX2 cells, normal fibroblasts and also transform macrophages into immuno-suppressive M2 state to promote pro-tumor functions. Overall, our findings identified a novel prognostic biomarker and treatment target for patients with CRC.

## Materials and methods

### Clinical specimens

All CRC and paired normal tissues were collected from patients who underwent surgery between 2019 and 2022 at the Sir Run Run Shaw Hospital (Hangzhou, Zhejiang, China). After surgery, tissue specimens were pathologically validated and preserved at  $-80^{\circ}\text{C}$  until further use. The stages of CRC tissues were classified according to the tumor-node-metastasis (TNM) staging system. Serum samples were also obtained from normal donors and patients with CRC at Sir Run Run Shaw Hospital. The Ethics Committee of Sir Run Run Shaw Hospital, Zhejiang University, approved this study.

### Extraction of exosomes

Exosomes were collected when CRC cells reached 80% confluence, and the medium was replaced with the exosome-free medium. The conditioned medium was collected after 2 days and extracted using differential centrifugation. The medium was first centrifuged at  $500 \times g$  for 15 min to remove cells, then at  $10,000 \times g$  for 30 min to remove cell debris. Ultracentrifugation was performed at  $120,000 \times g$  for 70 min at  $4^{\circ}\text{C}$ . The resulting pellet was resuspended in phosphate-buffered saline (PBS) and centrifuged again at  $120,000 \times g$  for 70 min to obtain pure exosomes. The concentration of extracted exosomes was measured using the BCA Protein Assay Kit (MeilunBio, Shenyang, China). The diameters and morphology of exosomes were assessed by transmission electron microscopy (TEM) (HT-7700, Hitachi).

### Cell lines and cell culture

Human CRC cell lines, including SW480, SW620, DLD1, HCT116, RKO, HT29, and LOVO, normal colonic epithelial cell line NCM460, LX2 and human macrophage cell line THP1 were obtained from the American Type Culture Collection (ATCC, Manassas, VA, USA). Human embryonic kidney cells (HEK-293T) were acquired from the Cell Bank of the Shanghai Academy of Chinese Sciences. Normal fibroblasts (NF) were isolated from tumor

colonic tissues of CRC patients. Cell lines were cultured in DMEM (Gibco) or RPMI 1640 medium (Gibco) with 10% fetal bovine serum (Gibco) and 1% penicillin-streptomycin and incubated at 37 °C with 5% CO<sub>2</sub>.

#### **RNA interference (RNAi) and plasmid transfection**

siRNAs targeting circSCP2 junction sites were obtained from RiboBio (Guangzhou, China) and transfected into RKO and LOVO cells using Lipofectamine RNAiMAX (Invitrogen, CA, USA). To create stable circSCP2 knockdown or overexpression, relative plasmids were obtained from GenePharma Co. Ltd., Shanghai, China. The sequences are listed in Table S1. Lentivirus was created in 293T cells using a Lenti-Pac HIV Expression package kit and Lipofectamine 3000 (Invitrogen, CA, USA) following the manufacturer's instructions. RKO, LOVO, HCT116 and SW480 cells were infected and treated with puromycin (Gibco, Grand Island, NY, USA) for several days to generate stable cells with circSCP2 knockdown or overexpression.

#### **RNA extraction and quantitative real-time PCR (qRT-PCR)**

Total RNA of cells or tissues was extracted using the SteadyPure RNA extraction Kit (AG21017, Accurate Biology, Changsha, China), following the manufacturer's instructions. After RNase R or actinomycin D treatment, RNAs were reverse transcribed into cDNA using the Evo M-MLV RT Premix kit following the manufacturer's instructions (Accurate Biology, Changsha, China). qRT-PCR was performed using the Hieff UNICON<sup>®</sup> qPCR SYBR<sup>®</sup> Green Master Mix (Yeasen, Shanghai, China) and a Roche LightCycler 480 II PCR instrument (Basel, Switzerland). circRNA and mRNA expression levels were normalized using  $\beta$ -actin. Relative RNA expressions were determined using the  $2^{-\Delta\Delta C_t}$  method. Primers are listed in Table S1.

#### **RNase R and actinomycin D treatment**

For RNase R treatment, total RNA was incubated with or without 3 U/ $\mu$ g RNase R (MedChemExpress, Shanghai, China) for 15 min at 37 °C. Cells undergoing relative transfections were treated with 5  $\mu$ g/mL actinomycin D (MedChemExpress, Shanghai, China) or DMSO and collected for RNA extraction at the indicated time points. The resulting RNA was reverse-transcribed and analyzed by qRT-PCR.

#### **RNA sequencing**

RKO cells transfected with siRNA-NC or siRNA-circSCP2 ( $n=3$ ) were used for RNA-seq, with analysis conducted by Majorbio (Shanghai, China).

#### **CCK8 (cell counting kit-8) and EdU (5-ethynyl-2'-deoxyuridine) assays**

CCK8 and EdU assays were performed to investigate the cell proliferation ability following different treatment. A total of 5000 cells resuspended in 100 $\mu$ L of medium containing 10% fetal bovine serum (FBS) was added to the 96-well plate. The OD values were read after 2-hour of addition of 10% CCK8 detection kit (MeilunBio, Shenyang, China) and continuously detected for 5 days. The EdU assays (C10310-1, RiboBio, Guangzhou, China) were performed following the manufacturer's instructions. The results were then photographed under a fluorescence microscope (DM IL LED, Leica, Germany). Each experiment was performed in triplicate.

#### **Transwell assay**

Migration and invasion assays were performed using transwell chambers (Corning, 3422, USA) precoated with or without Matrigel. A total of 50,000 cells resuspended in 100  $\mu$ L of serum-free medium were seeded in the transwell upper chamber, while 600  $\mu$ L of medium containing 10% fetal bovine serum (FBS) was added to the lower chamber. After 24 h, the invaded cells were fixed using 4% polymethanol for 20 min, stained with crystal violet (Sigma, MO, USA) for 30 min, and photographed under a microscope. Each experiment was performed in triplicate.

#### **Wound-healing assay**

When cells under different treatments reached 100% confluence, the cell monolayer was scratched using a 10  $\mu$ L pipette tip. To minimize the effects of cell proliferation, cells were cultured in a medium containing 1% FBS. Relative wound healing rates were calculated as the ratio of the migrated distance over relative times to the initial scratched width. Each experiment was performed in triplicate.

#### **Colony formation assay**

A total of 50,000 cells resuspended in 2mL of medium containing 10% fetal bovine serum (FBS) was added to the 6-well plate. The medium was changed every 2 days. After 7 days, the formed cell colonies were fixed using 4% polymethanol for 20 min, stained with crystal violet (Sigma, MO, USA) for 30 min, and photographed. Each experiment was performed in triplicate.

#### **Antibodies and western blotting**

Primary antibodies used were anti-E-cadherin (20874-1-AP, Proteintech), anti-N-cadherin (22018-1-AP, Proteintech), anti-MMP2 (AF5330, Affinity), anti-IGF2BP1 (22803-1-AP, Proteintech), anti-Vimentin (10336-1-AP, Proteintech), anti-PTBP1 (12582-1-AP, Proteintech), 67462-2-1 g, Proteintech), and anti-GAPDH

(60004-1-AP, Proteintech) antibodies. CRC cells were collected, washed, and lysed using RIPA lysis buffer (FD009, Fudebio, Hangzhou, China). Protein concentrations were quantified using a BCA Protein Assay Kit (MeilunBio, Shenyang, China). Proteins were separated by 8–12% SDS-PAGE and transferred to PVDF membranes (Millipore, Schwalbach, Germany). Membranes were blocked with TBST buffer containing 5% skim milk powder and incubated with the corresponding primary antibodies at 4 °C overnight. At room temperature, the membrane was hybridized for 1 h with an HRP-conjugated secondary antibody (FDM007 and FDR007, Fudebio, Hangzhou, China). The signals were detected using an enhanced chemiluminescence kit (FD8030, Fudebio, Hangzhou, China).

#### **RNA-protein immunoprecipitation (RIP) and RNA pulldown**

RIP analysis was performed using a Magna RNA-binding Protein Immunoprecipitation Kit (17–701, Merck Millipore, Bedford, MA, USA) following the manufacturer's instructions. RKO whole-cell lysates were prepared and incubated with anti-AGO2 antibody or negative control anti-IgG antibody (17–701, Merck Millipore, Bedford, MA, USA) at 4 °C overnight. Enriched RNAs were measured using qRT-PCR as described above and normalized to input samples.

The biotin-coupled RNA complex was pulled down using an RNA-protein pulldown kit (Bes5102, BersinBio, Guang Zhou, China) following the manufacturer's instructions. The 5' biotin-labeled oligonucleotide probe targeting the circSCP2 junction site was synthesized by GenePharma. Biotinylated circSCP2 was captured with streptavidin magnetic beads and incubated with cell lysates at 4 °C overnight. After purifying the immunoprecipitated proteins from the magnetic beads, the enriched proteins were analyzed using silver staining, western blotting, and liquid chromatography-mass spectrometry.

#### **Immunoprecipitation (IP) assay**

An anti-PTBP1 antibody (12582-1-AP, Proteintech) was used for the IP ubiquitination assay. To analyze the *in vitro* ubiquitination of circSCP2-overexpressing SW480 cells and circSCP2-knockdown RKO cells, MG132 was added for 6 h before protein collection. Proteins were incubated with Pierce Protein A/G Magnetic Beads (88802, Thermo Scientific™, USA) and anti-PTBP1 antibody overnight (12582-1-AP, Proteintech). The immune complexes were centrifuged and washed, and proteins were analyzed by western blotting with an anti-ubiquitin antibody (3936, Cell Signaling Technology) following the manufacturer's instructions.

#### **FISH (fluorescence in situ hybridization)**

The FAM (fluorescein amidite)-labeled circSCP2 RNA probe were designed and synthesized by Servicebio (Wuhan, China). To analyze the distribution of circSCP2

in CRC tumor tissues and cells lines, the FISH assays were performed using a Fluorescent In situ Hybridization Kit (RiboBio, Guangzhou, China) following the manufacturer's guidelines. Images were acquired using a fluorescence microscopy (Eclipse E6000; Nikon, Corporation, Tokyo, Japan).

HE (Hematoxylin and eosin), IHC (immunohistochemistry) and IF (immunofluorescence).

The tissues were embedded in paraffin and made into slices (4 μm). For H&E, paraffin was removed from slices with 3 times of xylene for 30 min, and slices were soaked in varying alcohol concentrations (from high to low). Then the slices were stained in a hematoxylin water solution for staining for 1 min, then decolorized with ammonia, alcohol, and distilled water successively. Finally, decolorized slices were sealed with resin and photographed. For the IHC assay, after the paraffin was removed from slices, the slices undergone antigen-repaired in Citrate Antigen Retrieval solution (Servicebio (Wuhan, China) and then 10% goat serum was added to the slices at room temperature for 1 h. Then, primary antibodies were added overnight at 4 °C. The secondary antibody was added to slices and incubated at room temperature for 2 h. Then the slices were subsequently treated with DAB, washing, hematoxylin stain, and washing. Finally, slices were sealed and captured under a microscope. For IF staining in cells, following fixation with 4% paraformaldehyde, cells were blocked using 10% goat serum. And the primary antibodies were added overnight at 4 °C. The secondary antibody and DAPI (4',6'-diamidino-2-phenylindole) was subsequently added to slices and incubated at room temperature for 2 h and 5 min, respectively. After addition of Antifade Mountant (Haoke, Hangzhou, China), images were acquired using a fluorescence microscopy (DM IL LED, Leica, Germany).

#### **Flow cytometry analysis**

After THP1 was stimulated into M0 state using 100 ng/ml of phorbosc-12-myristose-13-acetate (PMA) for 24 h, they were treated with the exosomes extracted from SW480 NC or SW480 circSCP2-OE cells for another 24 h. Then cells were digested and filtered through 40 μm meshes to generate single cell suspensions for subsequent flow cytometry analysis. Cells were subsequently stained with Fc block, Zoobie Violet™ Fixable Viability Kit (423114, Biolegend, San Diego, CA, United States), PE anti-mouse/human CD11b Antibody(101207, Biolegend, San Diego, CA, United States) and APC/Cyanine7 anti-human CD206 (MMR) Antibody(321120, Biolegend, San Diego, CA, United States). Analysis was conducted using a flow cytometer (CytoFlex S, Beckman Coulter, United States), and the data were processed and interpreted with FlowJo software (Tree Star) to assess cell populations and their activation states.

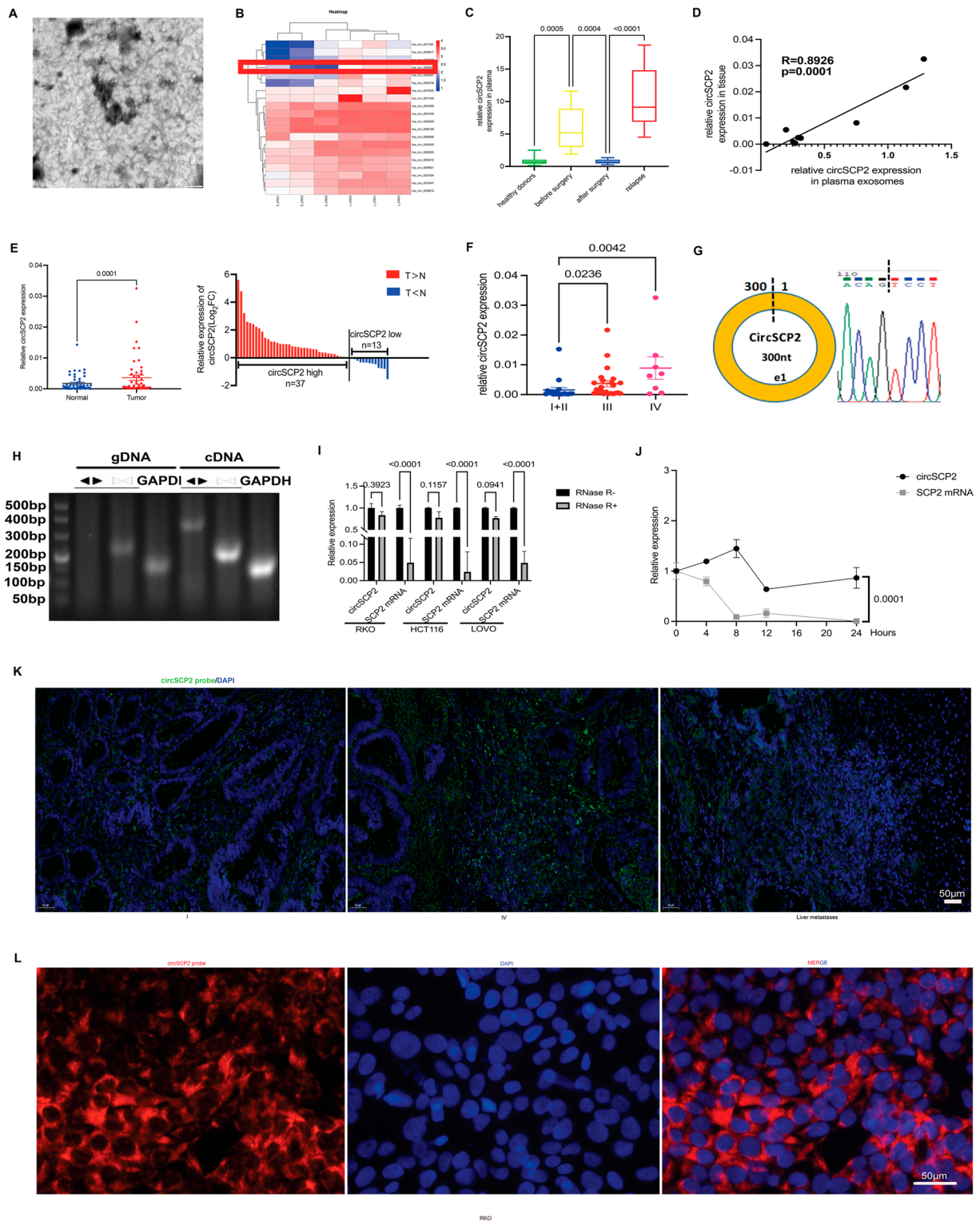


**Fig. 1** (See legend on next page.)

(See figure on previous page.)

**Fig. 1** Exosomal circSCP2 was enriched in CRC patients serum and tumor tissues. **(A)** Morphology and size of exosomes obtained from serum of patients with colorectal cancer under scanning electron microscope (SEM). Scale bar, 200  $\mu\text{m}$ . **(B)** Heat maps of differentially expressed circular RNAs obtained from exosomes of three pairs of patients with early and advanced colorectal cancer. **(C)** qRT-PCR analysis of circSCP2 mRNA expression in serum from healthy donors, patients before, after surgery as well as patients undergo relapse ( $N=10$  patients/group). **(D)** Correlation analysis of circSCP2 mRNA expression between patient plasma exosomes and tissues. **(E)** qRT-PCR analysis of circSCP2 mRNA expression within 50 pairs of normal and tumor tissues. **(F)** qRT-PCR analysis of circSCP2 mRNA expression within tissues from CRC patients under different stages. ( $N=50$  patients) **(G)** The schematic showed the circularization and back-splicing mode of SCP2 exon 1 to form circSCP2. The back-to-back splice junction site was confirmed by Sanger sequencing using the divergent primer. **(H)** Agarose gel electrophoresis of PCR product amplified from cDNA and gDNA of RKO cells using convergent and divergent primers. GAPDH was used as the negative control. **(I)** qRT-PCR analysis of circSCP2, linear SCP2 in RKO, HCT116 and LOVO cells with or without RNase R treatment. **(J)** CircSCP2 and linear SCP2 expression levels were detected after actinomycin D treatment in RKO cells. **(K)** FISH assays showed that the spatial distribution of circSCP2 was mostly present in tumor tissues and tumors with last stages and metastatic tumors such as liver metastases also showed extremely high expression of circSCP2. Scale bar, 50  $\mu\text{m}$ . **(L)** FISH assays showed that the sub-cellular distribution of circSCP2 was mostly present in the cytoplasm. Scale bar, 50  $\mu\text{m}$ . The data were independently repeated at least three times. Differences between two groups were analyzed using Student's t-tests

### Animal model

For the lung metastasis model,  $2 \times 10^6$  pretreated RKO cells were suspended in sterile PBS and injected intravenously into the tail veins of BALB/c nude mice (male, 4 weeks old). The LM model was established via intrasplenic injection of  $2 \times 10^6$  pretreated RKO cells. After approximately 1 month, the mice were anesthetized with isoflurane and intraperitoneally injected with 150 mg/kg D-luciferin (Yeason, Shanghai, China) for in vivo tumor imaging. After 15 min, tumor cells labeled by luminescence were imaged using a Spectrum in vivo imaging system (PerkinElmer, USA). Lung and liver tissues were harvested, fixed with phosphate-buffered formalin, and subjected to hematoxylin and eosin staining following the manufacturer's instructions.

### Statistical analyses

Statistical analyses were performed using the Statistical Package for the Social Sciences (version 25.0; SPSS Inc., Chicago, IL, USA) and GraphPad Prism (version 9; GraphPad, San Diego, CA, USA) software. Data are presented as the mean  $\pm$  standard deviation (SD) from at least three independent experiments. Differences between two groups were analyzed using Student's t-tests, while differences among multiple groups were calculated by one-way analysis of variance (ANOVA) with Dunnett's multiple comparisons test. Associations between circSCP2 expression and clinicopathological characteristics were evaluated using the Chi-square test. Detailed description of data, statistical methodology used, and sample size can be found at the end of the figure legend corresponding to each figure.

## Results

### circSCP2 is elevated in CRC tissues and patient serum exosomes

To identify potential circRNA candidates involved in CRC progression, we performed competing endogenous RNA (ceRNA) microarray sequencing to profile differentially expressed circRNAs in serum exosomes (Fig. 1A) from three patients with CRC and distant

metastases and three patients with CRC but without metastases. In total, 1,862 circRNAs were significantly expressed based on fold-change (FC) filtering ( $|\log_2\text{FC}| > 1$ ) and  $P\text{-value} < 0.05$ . To identify a promising prognostic circRNA critical during cancer progression, we randomly selected 5 circRNAs from the top 35 candidates (hsa\_circ\_0068545, hsa\_circ\_0009071, hsa\_circ\_0073014, circSCP2, and hsa\_circ\_0082968) with significantly high expression based on raw abundance signals and FCs. We then used quantitative real-time PCR (qRT-PCR) to determine their expression levels in 10 pairs of CRC tissues from patients (Figures S1A–E). Only circSCP2 was significantly upregulated in tumor tissues compared with normal tissues. circSCP2 was selected for further investigation as it was one of the most upregulated non-coding RNAs in our microarray data (7.78-fold change) (Fig. 1B).

Next, we used qRT-PCR to detect and analyze plasma circSCP2 expressions in healthy donors, patients before and after surgery, and patients with recurrent cancer. Plasma circSCP2 expression was significantly upregulated in relapsed and preoperative patients (Fig. 1C). We also discovered a positive correlation between serum exosomal and cancer tissue circSCP2s (Fig. 1D). Western blotting was used to analyze the exosome markers TSG101, CD63, and CD81 (Figure S1F). In 50 paired CRC tissues and corresponding normal tissues, 37 pairs of cancer tissues exhibited elevated circSCP2 expression, while 13 pairs exhibited decreased circSCP2 expression (Fig. 1E). We also discovered that circSCP2 expression increased with cancer progression (Fig. 1F). No significant differences were observed in circSCP2 expression in paired normal fibroblasts (NAFs) and carcinoma-associated fibroblasts (CAFs) (Figure S1G). Overall, we hypothesized that circSCP2 played a critical role in tumor development.

According to the circBase database, circSCP2 (chr1:53459074–53459374) is 300 base pairs long and is derived from the sterol carrier protein 2 (SCP2) gene (Fig. 1G). Gel electrophoresis confirmed the circular characteristic of circSCP2 (Fig. 1H), and Sanger sequencing confirmed its existence and back-splicing position (Fig. 1G). To assess circSCP2 stability, RKO, HCT116, and

LOVO cells were treated with RNase R, and qRT-PCR results exhibited that circSCP2 was more stable than linear SCP2 transcripts (Fig. 1I). Additionally, circSCP2 was resistant to actinomycin D treatment compared with the linear SCP2 (Fig. 1J). To identify circSCP2 expression in CRC tissues, we performed FISH assays. Consistent with qRT-PCR results, circSCP2 was significantly overexpressed in CRC tissues compared with normal tissues. Advanced (CRC tissues at stage III or IV) and metastatic tumors also exhibited higher circSCP2 expressions. Tumor stroma also expressed elevated circSCP2 (Fig. 1K). Overall, exosomal circSCP2 may orchestrate tumor microenvironments during tumor progression. The FISH assay was also performed to determine the subcellular circSCP2 distribution in RKO cells, and the majority of circSCP2 was preferentially localized in the cytoplasm (Fig. 1L). Clinical data from 50 cases revealed that circSCP2 expression was significantly correlated with tumor stage and lymph node invasion (Table S1). In summary, our data indicate that circSCP2 is upregulated in CRCs and is strongly associated with tumor progression and metastasis.

#### **circSCP2 promotes the proliferation, invasion and metastasis of CRC**

To evaluate the biological function of circSCP2 *in vitro*, we used qRT-PCR to assess its expression levels in normal human intestinal epithelial cells (NCM460 cells) and CRC cells (SW480, SW620, Colo320, HCE8093, DLD1, HCT116, RKO, LOVO). HCT116, RKO and LOVO cells exhibited significantly higher circSCP2 expression levels than NCM460 cells (Fig. 2A). Then, we chose RKO and LOVO cells for further investigation. Three small interfering RNAs (siRNAs) were designed and transfected into RKO and LOVO cells, and qRT-PCR analysis validated that si-circSCP2#1 and si-circSCP2#3 significantly decreased circSCP2 expression. Therefore, si-circSCP2#1 and si-circSCP2#3 were used to investigate circSCP2 function *in vitro* (Fig. 2B). CCK8 and EdU assays revealed that circSCP2 knockdown inhibited CRC cell proliferation (Fig. 2C-D). Wound healing assays revealed that reducing circSCP2 expression significantly suppressed CRC cell migration (Fig. 2E). Transwell assays indicated that reduced circSCP2 expression significantly reduced CRC cell migration and invasion abilities (Fig. 2F). Plate colony formation assay results similarly demonstrated that circSCP2 depletion decreased cell proliferation (Fig. 2G). These results indicated that circSCP2 significantly affected CRC cell proliferation, migration, and invasion.

The role of circSCP2 *in vivo* was then investigated. RKO cells stably transfected with sh-circ#1 or a control vector were injected subcutaneously into nude mice. Consistent with the *in vitro* results, circSCP2 knockdown significantly decreased tumor volume and growth rate (Fig. 3A-B). Furthermore, RKO cells transfected with sh-circ#1

or a control vector were injected into the tail vein and spleen to create lung metastasis and LM models, respectively. HE staining revealed that mice injected with circSCP2-knockdown RKO cells exhibited smaller and fewer metastatic tumor nodules in the lungs (Fig. 3C-D) and livers (Fig. 3G-H). IHC staining also showed expressions of EMT-related proteins including N-cadherin and Vimentin were decreased in the lung and liver metastase (Fig. 3E-I). Quantitative analysis of metastases and luminescence in the lung metastasis and liver metastasis of mice models also confirmed decreased metastases in mice injected with circSCP2-knockdown RKO cells (Fig. 3F-J). These results confirmed that circSCP2 could play an oncogenic role in CRC by promoting invasion and metastasis.

#### **circSCP2 serves as a sponge for miR-92a-1-5p**

Given that the predominant function of circRNA is miRNA sponging, we investigated whether circSCP2 could bind to miRNAs and mediate CRC metastasis. Overlapping predictions from three databases (miRanda, Targetscan, and RNAhybrid) identified 26 miRNAs that might probably bind to circSCP2 (Fig. 4A). Based on expression levels and prognosis of these 26 miRNAs predicted by Targetscan, only miR-26-3p and miR-92a-1-5p were downregulated in CRC. To validate the miRNA candidates, we conducted a dual-luciferase reporter assay. When miR-92a-1-5p mimics were cotransfected with the circSCP2 wild-type dual-luciferase reporter plasmid, luciferase activity was significantly reduced compared with NC mimics, whereas miR-26-3p mimics exhibited no effect. In contrast, the luciferase activity of circSCP2 mutant dual-luciferase reporter plasmid was unaffected by miR-92a-1-5p mimics (Fig. 4B). Most studies revealed that argonaute 2 (AGO2) is the core component of the miRNA-induced silencing complex, which plays an important role in tumorigenesis and invasion. We performed a biotin-labeled RNA pulldown assay (RIP), which confirmed that circSCP2 was significantly enriched in RKO cells overexpressing miR-92a-1-5p obtained with the anti-AGO2 antibody (Fig. 4C). Targetscan predicted that miR-92a-1-5p expression is decreased in CRC tissues (Fig. 4D). Consistently, we confirmed that miR-92a-1-5p expression in CRC tissues was negatively correlated with circSCP2 (Fig. 4E). Additionally, FISH assays demonstrated colocalization of circSCP2 and miR-92a-1-5p in the cytoplasm (Fig. 4F). The results suggested that circSCP2 can directly bind to miR-92a-1-5p. The results of qRT-PCR confirmed that RKO and LOVO cells transfected with sh-circ#1 exhibited the lowest circSCP2 expression, so we used sh-circ#1 plasmid for circSCP2 expression knockdown in subsequent experiments (Figure S2A). CCK8 assays revealed that circSCP2 knockdown decreased the proliferation of RKO and LOVO cells, which were inhibited by miR-92a-1-5p inhibitor (Figures S2B-C). Wound healing and transwell assays further demonstrated that

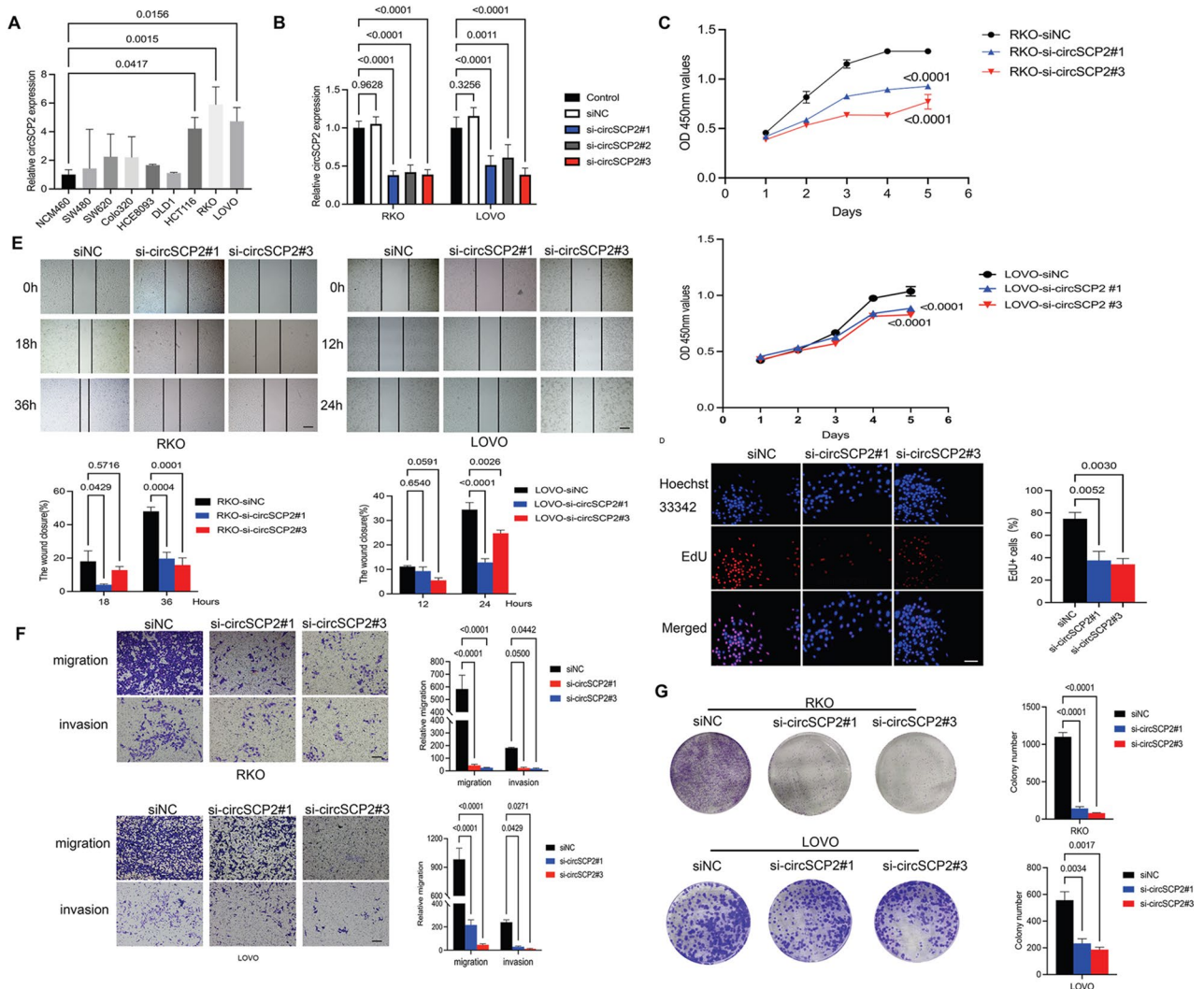


**Fig. 2** Knockdown of circSCP2 suppressed proliferation, invasion and migration of CRC cells. **(A)** qRT-PCR analysis of circSCP2 mRNA expression among normal colonic epithelial cells (NCM460) and CRC cells (SW480, SW620, Colo320, HCE8093, DLD1, HCT116, RKO, LOVO). **(B)** qRT-PCR analysis was used to evaluate the transfection efficiency of three types of siRNAs in colorectal cancer cells (RKO and LOVO cells). **(C)** CCK8 assays and **(D)** EdU analysis were used to determine the growth ability of CRC cells after knocking down the expression of circSCP2 relative to the negative control group. **(E)** Wound healing assays were used to evaluate the effect of circSCP2 knockdown on the invasion ability of RKO and LOVO cells. **(F)** Transwell experiments were used to evaluate the effect of circSCP2 knockdown on the migration and invasion ability of RKO and LOVO cells. **(G)** Colony formation assays were conducted to evaluate the proliferation ability of CRC cells after knocking down of circSCP2. The data were independently repeated at least three times. The results were presented as the means  $\pm$  SD. Data were compared using one-way ANOVA with Dunnett's multiple comparisons test

miR-92a-1-5p inhibitor significantly mitigated the inhibitory effect of circSCP2 knockdown CRC cell migration and invasion (Fig. 4G-H and Figure S2D-E). Similar results were observed in colony formation assays (Figure S2F).

#### circSCP2 inhibits miR-92a-1-5p-induced silencing of IGF2BP1

Using RNA-seq, we analyzed the altered mRNA following circSCP2-knockdown. Gene ontology (GO) enrichment analysis demonstrated that circSCP2 suppression significantly affected extracellular matrix (ECM) construction, angiogenesis, and cell adhesion, indicating

a strong correlation between circSCP2 and metastasis (Fig. 5A). Additionally, GSEA analysis confirmed a positive correlation between circSCP2 expression and EMT (Fig. 5B). To identify downstream targets through which circSCP2 functions as a miRNA sponge for miR-92a-1-5p, we used TargetScan, miRNA-walk, and miRDB with our RNA-seq results, and IGF2BP1 and PPFIA were identified as potential candidates (Fig. 5C). qRT-PCR analysis revealed that transfections with miR-92a-1-5p mimics and inhibitors significantly reduced IGF2BP1 mRNA expression compared with the control group (Fig. 5D). However, regardless of transfection, PPFIA4 expression

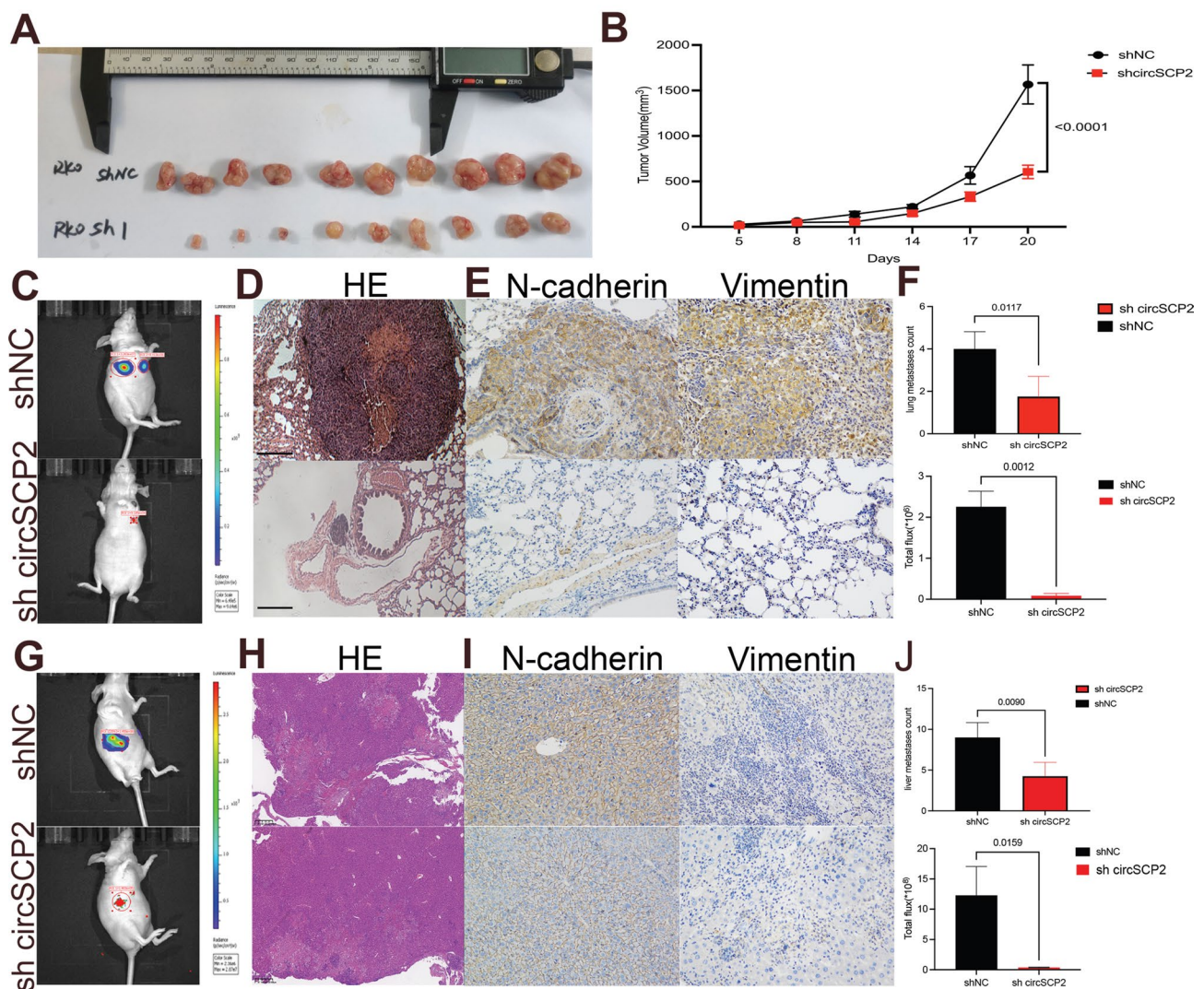


**Fig. 3** knockdown of circSCP2 inhibited the growth and metastasis of RKO cells in vivo. **(A)** Tumor size and **(B)** growth of the subcutaneous tumor growth model injected with RKO cells ( $n = 10$  mice/group). **(C)** Representative images and **(D)** relative HE staining of lung metastasis of mice using luciferase-based bioluminescence imaging. **(E)** IHC analysis of N-cadherin and Vimentin in lung metastasis of mice ( $n = 4$  mice/group). **(F)** Quantitative analysis of lung metastases and luminescence in the lung metastasis mice models. **(G)** Representative images and **(H)** relative HE staining of liver metastasis of mice using luciferase-based bioluminescence imaging. **(I)** IHC analysis of N-cadherin and Vimentin in liver metastasis of mice. **(J)** Quantitative analysis of liver metastases and luminescence in the liver metastasis mice models ( $n = 4$  mice/group). Scale bar, 400  $\mu\text{m}$ . The results were presented as the means  $\pm$  SD. Data were compared using Student's t-tests

in miR-92a-1-5p mimics or inhibitors exhibited no significant changes (Fig. 5D). We also confirmed that IGF2BP1 mRNA expression was positively correlated with circSCP2 in our CRC tissues (Fig. 5E). Similarly, IGF2BP1 protein levels in CRC cells were inhibited by miR-92a-1-5p mimics and upregulated by miR-92a-1-5p inhibitors (Fig. 5F). Furthermore, miR-92a-1-5p inhibitors could significantly reverse the decreases in N-cadherin, IGF2BP1, and Vimentin expression caused by circSCP2 knockdown while inhibiting the reduction in E-cadherin expression (Fig. 5G). These data indicate that circSCP2 can inhibit miR-92a-1-5p-induced IGF2BP1 downregulation.

#### circSCP2 interacts with PTBP1 in CRC cells

We used four algorithms (circAtlas, RBPDB, StarBase, and catRAPID) to predict candidate circSCP2-associated RBPs because circRNA can bind to specific RBPs to exert their functions. PTBP1 and IGF2BP1 were identified as putative sponging RBPs for circSCP2 (Fig. 6A). The direct interaction between circSCP2 and predicted RBPs was verified through protein pull-down assays using biotin-labeled NC or circSCP2 sense probes, followed by silver staining and western blotting (Fig. 6B-C). PTBP1 was observed to interact with circSCP2, while HuR exhibited minimal binding (Fig. 6C). Additionally, PTBP1 was identified in the circSCP2 pull-down using liquid chromatography-mass

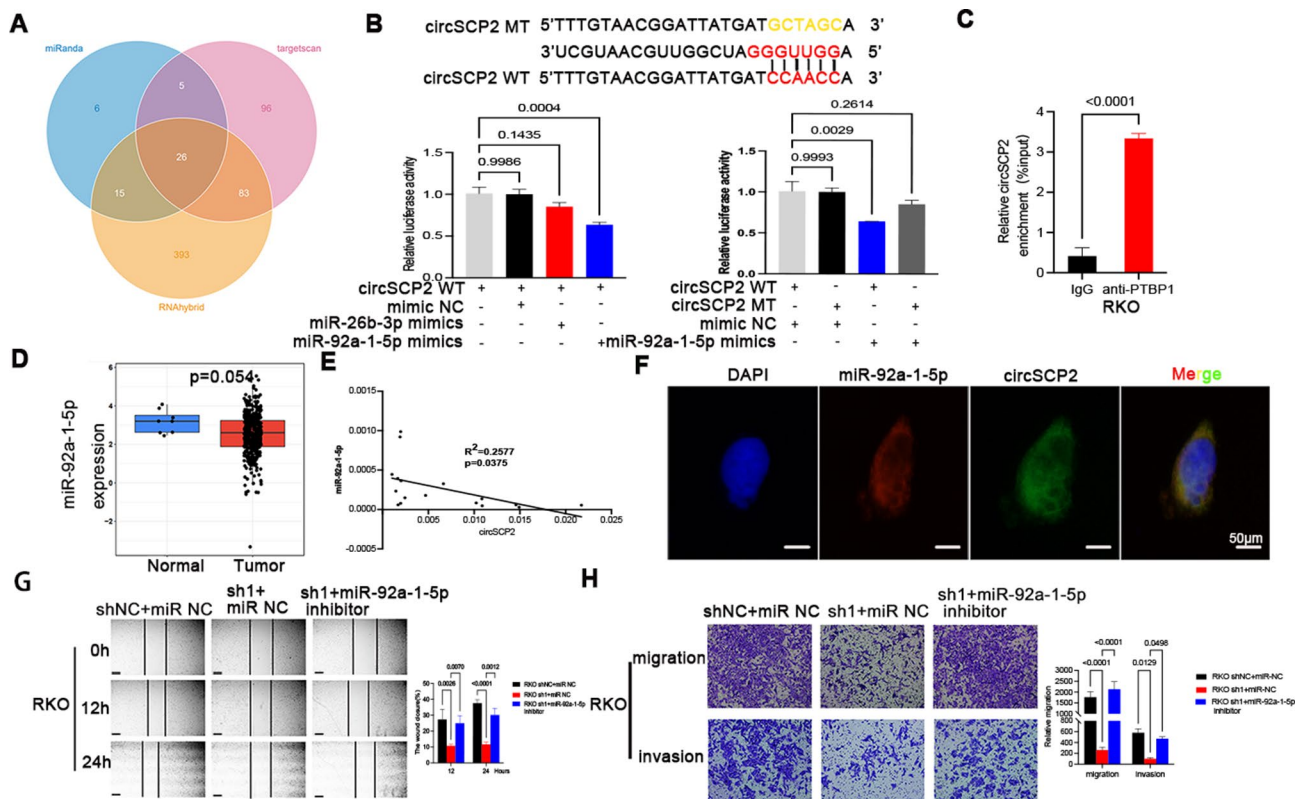


**Fig. 4** circSCP2 functioned as a miR-92a-1-5p sponge to promote cancer cell function. **(A)** Venn diagram showed the intersection of miRNAs predicted by the 3 online databases (miRanda, targetsScan, RNAhybrid). **(B)** The sequence alignment of circSCP2-WT and circSCP2-MT in luciferase reporter assay for validating the binding of circSCP2 and miR-92a-1-5p. Luciferase reporter assay showing the luciferase activity of the circSCP2 luciferase reporter plasmid (WT or MUT) following transfection with miR-NC or miR-92a-1-5p or miR-26b-3p mimic into HEK-293T cells. **(C)** Ago2-RIP assay was applied to detect the enrichment of circSCP2 in RKO cells transfected with miR-92a-1-5p mimics. **(D)** Expression of miR-92a-1-5p in CRC tissues and normal tissues in TCGA database was obtained from TargetsCan. **(E)** Existence of positive linear correlation between miR-92a-1-5p expression and circSCP2 in CRC tissues. **(F)** RNA FISH detection of circSCP2 and miR-92a-1-5p co-expression in the cytoplasm of RKO cells. Scale bar, 50  $\mu\text{m}$ . **(G)** Wound healing analysis and **(H)** Transwell assays detected the survival effect on the invasion and migration ability of circSCP2-knockdown CRC cells after transfection of miR-92a-1-5p inhibitors. The results were presented as the means  $\pm$  SD. Data were compared using one-way ANOVA with Dunnett's multiple comparisons test

spectrometry (LC-MS/MS) (Table S2). qRT-PCR analysis further demonstrated that circSCP2 was significantly enriched in PTBP1 RIP compared with the IgG RIP, indicating the interaction between PTBP1 and circSCP2 (Fig. 6D). To identify PTBP1 protein expression, we constructed CRC cells with circSCP2 overexpression or knockdown. While PTBP1 mRNA levels remained unchanged with circSCP2 overexpression or knockdown (Fig. 6E), PTBP1 protein levels were positively correlated with circSCP2 expression (Fig. 6F). These findings indicate that circSCP2 may stabilize PTBP1 protein post-transcriptionally. To test this hypothesis, circSCP2-knockdown RKO cells and circSCP2 OE (circSCP2-overexpressing) SW480 cells were treated with CHX (cycloheximide) to inhibit protein synthesis for the indicated periods. The results demonstrated that overexpression of circSCP2 significantly reduced the PTBP1 degradation rate. When compared with lysosome inhibitor chloroquine cotreatment, cotreatment with the proteasome inhibitor MG132 significantly reversed PTBP1 degradation, suggesting that

circSCP2 likely prevented PTBP1 degradation through the ubiquitination/proteasome system (Fig. 6G). To further test this hypothesis, we measured PTBP1 ubiquitination in circSCP2 OE SW480 cells and circSCP2 knockdown RKO cells. As displayed in Fig. 6H, PTBP1 ubiquitination decreased relatively after circSCP2 OE compared with the NC groups, while increased ubiquitination was observed in PTBP1 immunoprecipitation from circSCP2 knockdown groups (Fig. 6H). Overall, circSCP2 interacted with PTBP1 and promoted PTBP1 protein stability by inhibiting ubiquitination/proteasome-dependent degradation.

#### circSCP2 acts as scaffold to stabilize IGF2BP1 mRNA via interaction with PTBP1

PTBP1, recognized as an RNA-binding protein with oncogenic properties, directly binds to RNAs, mediating their stability and translation. Given that circSCP2 could bind to PTBP1, we speculated that circSCP2 might modulate mRNA stability by interacting with PTBP1 in CRC. To identify downstream targets of PTBP1, we

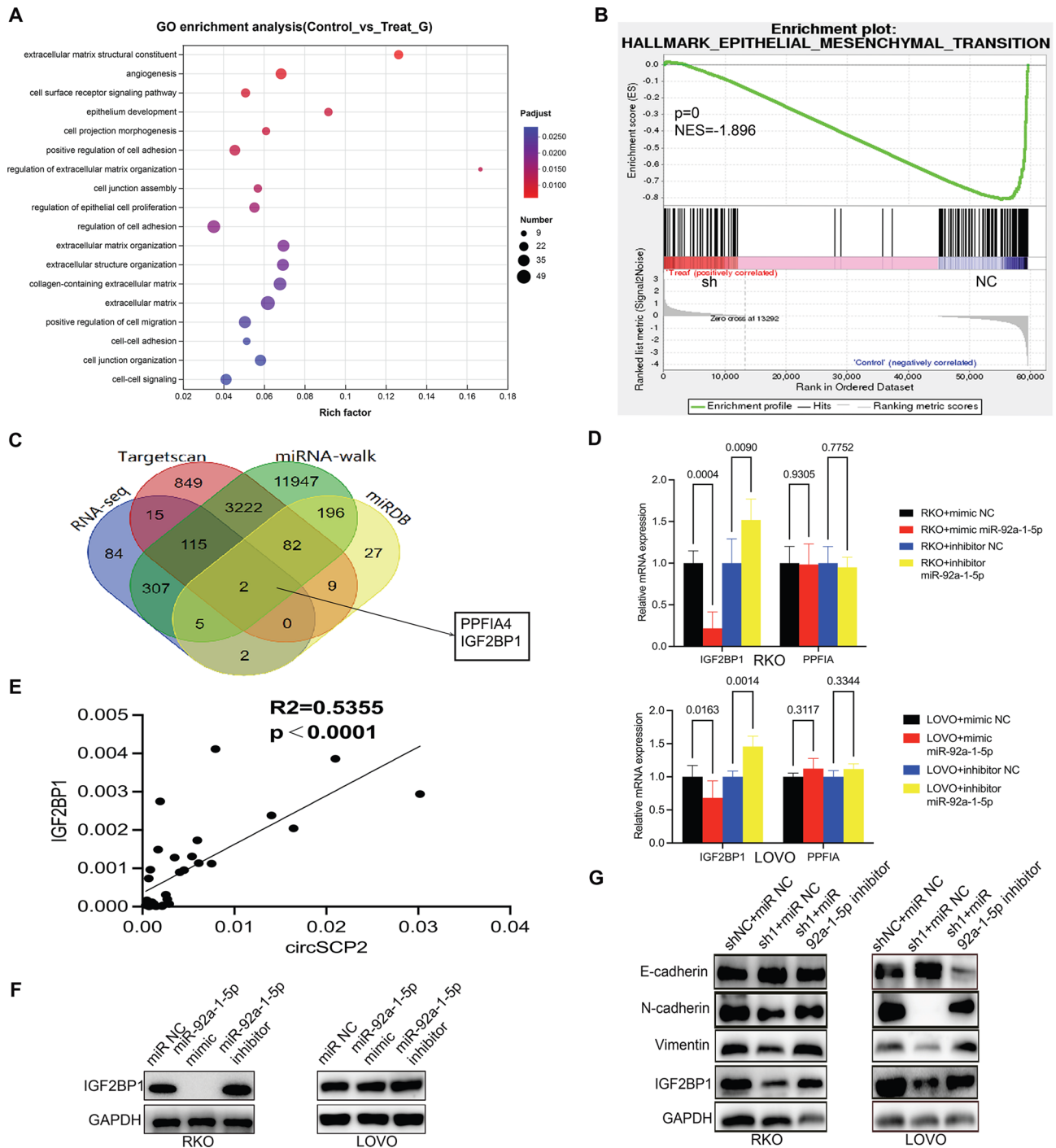


**Fig. 5** circSCP2 promoted EMT of CRC cells via sponging miR-92a-1-5p/IGF2BP1 axis. **(A)** Bubble diagram of GO pathway analysis between control and sh-circSCP2 RKO cells showed the enriched pathways. **(B)** GSEA analysis showed that expression of circSCP2 was positively correlated with EMT progress. **(C)** Venn diagram showed the intersection of downstream target of miR-92a-1-5p predicted by the RNA-seq results and 3 online databases (Target scan, miRNA-walk, miRDB). **(D)** qRT-PCR analysis of IGF2BP1 and PPFIA mRNA expression in RKO and LOVO cells after inhibition or overexpression of miR-92a-1-5p. The results were presented as the means  $\pm$  SD. Data were compared using one-way ANOVA with Dunnett's multiple comparisons test. **(E)** Positive correlation between circSCP2 and IGF2BP1 obtained from CRC patients. **(F)** Western blotting of IGF2BP1 protein expression in RKO and LOVO cells after inhibition or overexpression of miR-92a-1-5p. **(G)** Western blotting confirmed that transfection of miR-92a-1-5p inhibitor could rescue the EMT-related proteins and IGF2BP1 protein expressions after knocking down circSCP2 expression. Data were compared using one-way ANOVA with Dunnett's multiple comparisons test

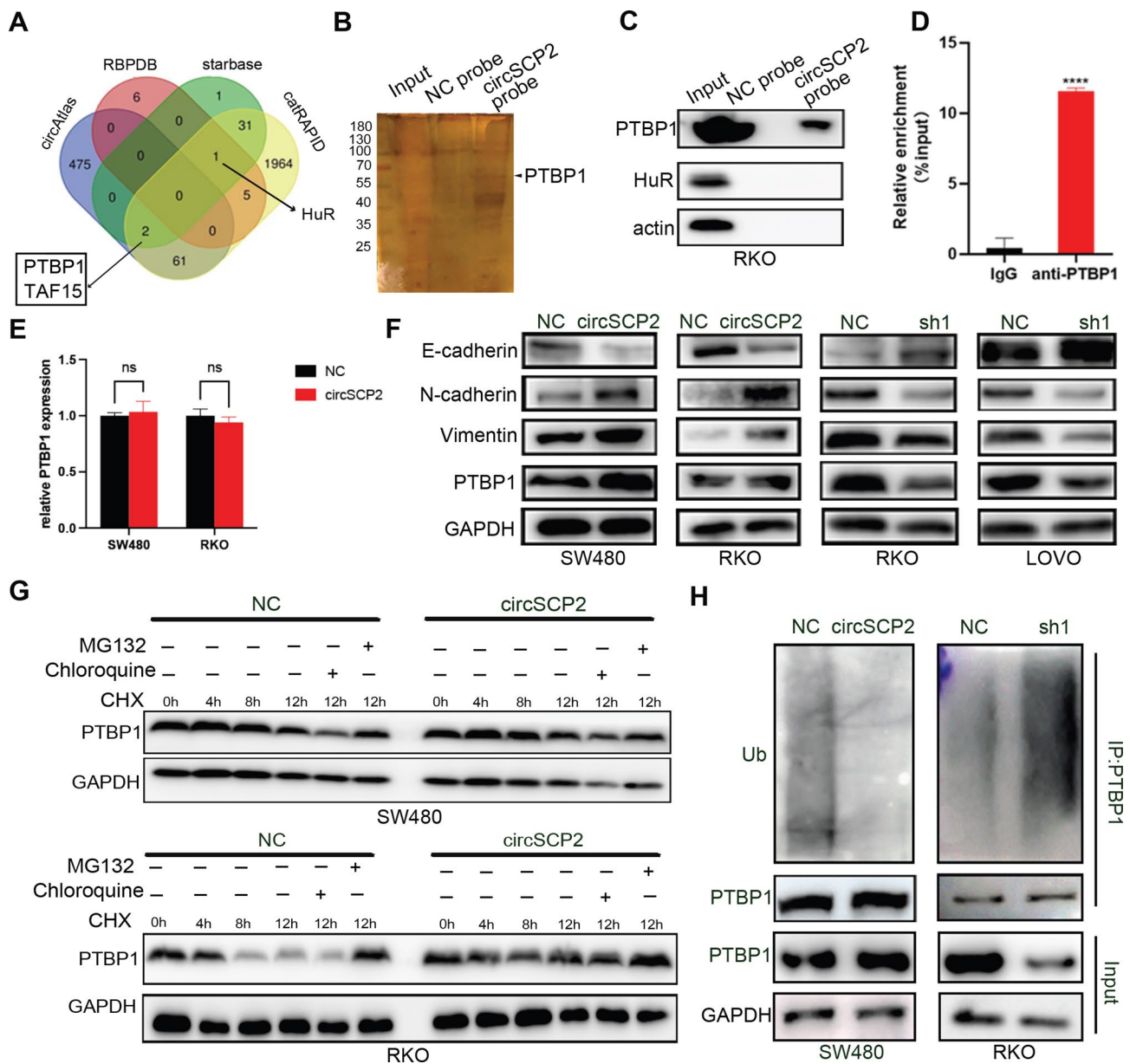


**Fig. 6** circSCP2 interacted with PTBP1 and regulated its ubiquitination-induced degradation in CRC cells. **(A)** Venn diagram showed the intersection of RBPs predicted by the 4 online databases (circAtlas, RBPDB, starbase and catRAPID). **(B)** Silver-stained SDS-PAGE gel-containing proteins derived from RNA pull-down by circSCP2 probe and negative control. **(C)** Western blotting analysis of protein precipitates obtained from RNA pull-down by circSCP2 probe and negative control. **(D)** qRT-PCR analysis of circSCP2 expression in anti-PTBP1 antibody-incubated precipitation relative to anti-IgG negative control. **(E)** qRT-PCR analysis of PTBP1 mRNA expression in circSCP2 OE SW480 and RKO cells. **(F)** Western blotting analysis of PTBP1 protein and EMT-related proteins including E-cadherin, N-cadherin and Vimentin in circSCP2 OE (SW480 and RKO) cells as well as circSCP2-knockdown (RKO and LOVO) cells. **(G)** Western blotting analysis of PTBP1 protein in control and circSCP2-knockdown RKO cells as well as circSCP2 OE SW480 cells treated with CHX treatment. **(H)** Ubiquitination modification of PTBP1 proteins in circSCP2 OE SW480 cells and circSCP2-knockdown RKO cells was determined via Co-IP and western blotting. Data were compared using Student's t-test

analyzed previously published CLIP-sequencing data on PTBP1-interacted proteins from POSTAR and Starbase. Seven proteins were identified at the intersection of these sequencing and the RNA-seq mentioned above (Fig. 7A). Among these seven proteins, we investigated whether circSCP2 interacted with IGF2BP1 and subsequently stabilized its mRNA. According to our hypothesis, ectopic

PTBP1 expression significantly prolonged the half-life of IGF2BP1 mRNA, while circSCP2 inhibition decreased IGF2BP1 mRNA stability (Fig. 7B). IF assays were performed to assess the PTBP1 and IGF2BP1 subcellular localization and expression in circSCP2 OE SW480 cells (Fig. 7C), which indicated the colocalization of PTBP1 and IGF2BP1. Transwell assays indicated that circSCP2

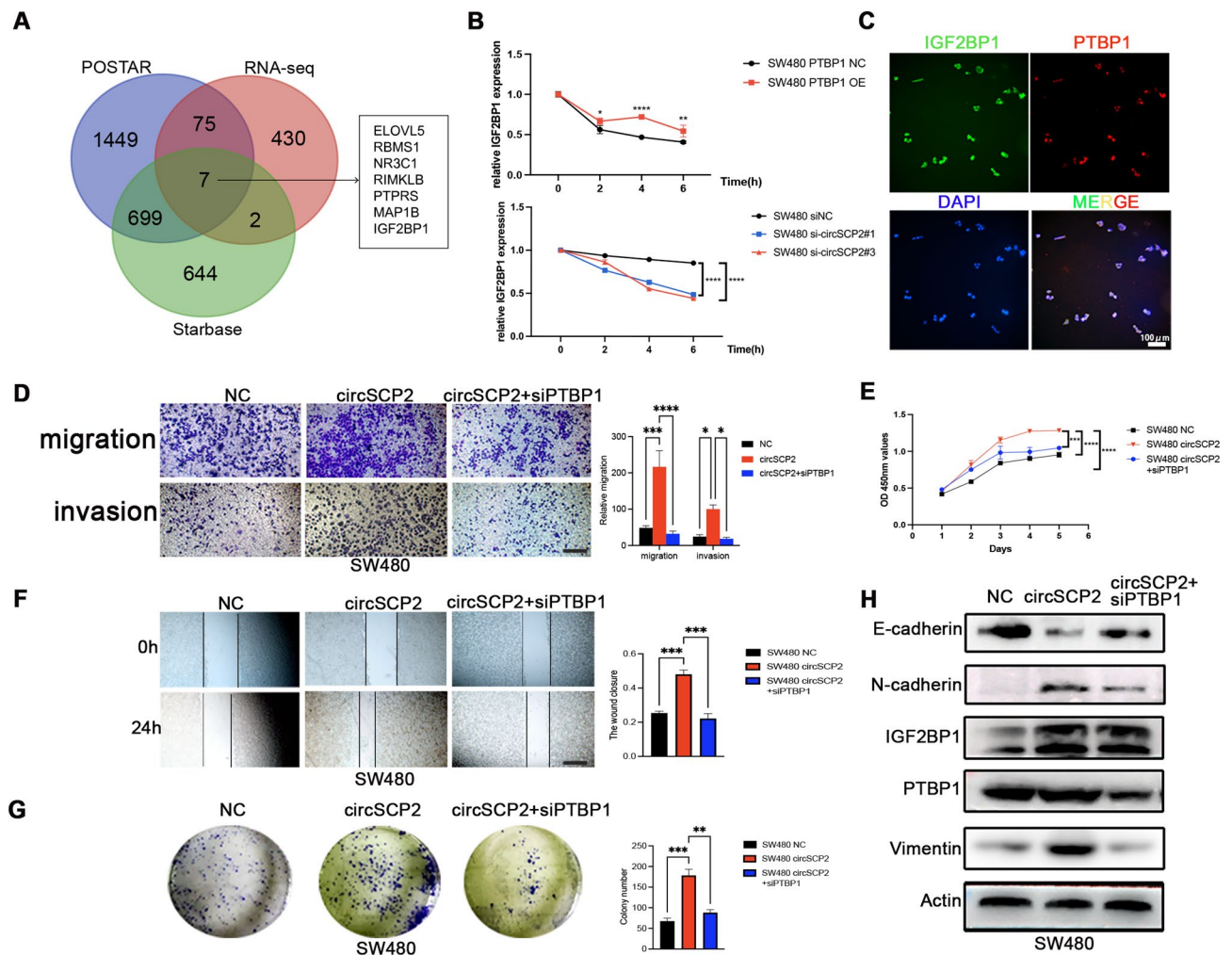


**Fig. 7** CircSCP2 interacted with PTBP1 and stabilized IGF2BP1 mRNA expression. **(A)** Venn diagram showed the downstream target of PTBP1 using overlap of predictions from 2 published databases including POSTAR and starbase, and the results of RNA-seq. **(B)** qRT-PCR analysis of IGF2BP1 mRNA expression in PTBP1 OE and circSCP2-knockdown SW480CRC cells. **(C)** IF analysis showed that the colocalization of PTBP1 and IGF2BP1 in RKO cells. Scale bar, 20  $\mu$ m. **(D)** Transwell experiments, **(E)** CCK8 assays, **(F)** wound healing assays, **(G)** colony formation experiments were used to evaluate the effect of PTBP1 knockdown on the migration, invasion and proliferation ability of circSCP2 OE SW480 cells. **(H)** Western blotting were used to evaluate the effect of PTBP1 knockdown on the expressions of EMT-associated proteins as well as IGF2BP1 within the circSCP2 OE SW480 cells. Data were compared using one-way ANOVA with Dunnett's multiple comparisons test

overexpression significantly enhanced CRC cell migration and invasion abilities, while suppression of PTBP1 expression inhibited circSCP2-induced tumor-promoting functions (Fig. 7D). CCK8 revealed that knockdown of PTBP1 inhibited circSCP2-induced upregulation of CRC cell proliferation (Fig. 7E). Wound healing assays revealed that reducing PTBP1 expression significantly suppressed circSCP2-induced upregulation of CRC cell migration (Fig. 7F). Plate colony formation assay results similarly demonstrated that PTBP1 depletion on the circSCP2 OE SW480 cells decreased cell proliferation (Fig. 7G). Results of western blot also indicated that PTBP1-knockdown on circSCP2 OE SW480 cells significantly suppressed EMT-related proteins (E-cadherin, N-cadherin and Vimentin) as well as IGF2BP1 expressions (Fig. 7H).

### Exosomal circSCP2 could modulate tumor-stroma microenvironment

Exosomes are well-known for their pivotal roles in cell-cell communication [4, 8]. Given the significant circSCP2 expression within tumor stroma and the vital impacts of circSCP2 on EMT progress, we investigated whether tumor-secreted exosomal circSCP2 could be transmitted into surrounding normal fibroblasts, subsequently inducing CAF activation. LX2 cells, a CAF precursor cell, were treated with condition medium (CM) or exosomes derived from circSCP2-overexpressing SW480 cells. Compared with untreated, treatment with either CM or exosomes significantly enhanced collagen constricting and proliferation abilities (Figures S3A-B). qRT-PCR results indicated that treatment with CM or

exosomes from circSCP2 OE SW480 cells increased circSCP2 expression in LX2, verifying that exosomal circSCP2 could be uptaken by LX2, leading to their activation (Figure S3C). To further demonstrate the cell morphology and activation state, phalloidin and ACTA2 were stained using the IF assays. Consistent with previous findings, normal fibroblasts treated with exosomes from circSCP2 OE SW480 cells exhibited elongated and activated morphology similar to CAFs. Similarly, LX2 treated with exosomes from sh-circ#1 RKO cells reverted to a resting state (Figure S3D). These results reveal that exosomal circSCP2 may also participate in tumor-stroma communications, orchestrating tumor progression. It is well-known that immune system played an important biological role in tumor progression [13]. The immunosuppressive tumor microenvironment, in which tumor-associated macrophages (TAMs) play important roles in the metastasis and drug resistance of cancer [14]. TAMs primarily consist of pro-inflammatory M1 and anti-inflammatory M2 macrophages, and multiple reports have discovered that M2 macrophages could promote tumor progression [13–15]. Therefore, we also explored whether exosomes containing circSCP2 could promote polarization fate of M2 macrophages. To further examine whether exosomal circSCP2 is valuable for M2 macrophage polarization and recruitment, we performed coculture of THP1 cells with NC or circSCP2 OE exosomes after induction of M0 THP1 cells with PMA (Phorbol 12-myristate 13-acetate) for 24 h. Co-culture with exosomes extracted from SW480 circSCP2 OE cells upregulated M2 macrophages markers, CD206 and IL-10 mRNA levels (Figure S3E) and upregulated proportions of CD11b<sup>+</sup>CD206<sup>+</sup> M2 macrophages (Figure S3F). Other hand, SW480 circSCP2 OE cells showed reduced sensitivity to chemotherapy Oxaliplatin, which further indicates the notion that targeting circSCP2 may be a new tumor therapeutic target (Figure S3G).

## Discussion

CRC has the third highest morbidity among tumors, with metastasis being the main cause of death [16]. circRNAs are recognized as critical mediators in tumorigenesis of various cancers, including CRC [4, 6]. Numerous studies have explored circRNA functions in CRC development and their potential as diagnostic and prognostic biomarkers [4, 6]. Our study discovered that circSCP2 was significantly upregulated in CRC tissues and serum exosomes. Additionally, serum exosomal circSCP2 expression increased with CRC progression. Further analysis revealed that high circSCP2 expression was associated with poor prognosis in patients with CRC and could promote CRC cell progressive and invasive behaviors.

Dysregulated circRNAs are well known to coordinate cancer progression; however, the underlying mechanisms

remain unclear. Extensive studies have revealed that circRNAs sponge or sequester miRNAs, thereby relieving miRNA-mediated suppression of target mRNAs [6, 17]. Ma et al. demonstrated that circPTPN22 modulates autophagy and other biological functions in gastric cancer via the miR-6788-5p/PAK1 axis [18]. Similarly, circPDIA3 served as a miR-449a sponge to regulate XBP1 expression, which inhibits palmitoylation of the GSDME-C domain, inducing chemoresistance in CRC [19]. In our study, both in vitro and in vivo experiments indicated that circSCP2 knockdown in CRC cells suppressed EMT and metastasis. Notably, circSCP2 indirectly regulated IGF2BP1 expression by sponging miR-92a-1-5p, a member of the miR-17-92 cluster, which is among the most characterized oncogenic miRNAs [20, 21]. However, miR-92a-1-5p expression in CRC tissues was lower than that in normal tissues in the TCGA database. Hou and colleagues discovered that NGF overexpression in osteosarcoma promoted MMP-2-dependent cell migration by inhibiting miR-92a-1-5p effects via the MEK/ERK signaling cascade [22]. Similarly, Yu et al. reported downregulated miR-92a-1-5p expression in circulating exosomes from patient serum [23], a finding also observed in exosomes from patients with prostate cancer [24]. Consequently, the related mechanism of miR-92a-1-5p requires further investigation.

Accumulating studies reveal that circRNAs participated in post-transcriptional regulation by recruiting RBPs to exert significant biological effects [11, 12, 17]. In our research, cytoplasmic circSCP2 interacted with PTBP1, enhancing its protein expression by inhibiting ubiquitination-induced degradation. PTBP1, an RNA-binding protein known for its function in regulating mRNA stability, further increased IGF2BP1 mRNA stabilization. IGF2BP1, an N6-methyladenine (m6A) binding protein, modulates over 3,000 mRNA transcription targets, including the PTEN, ACTB, MAPK, cMyc, and CD44, thereby regulating cell proliferation, tumor growth, invasion, and chemotherapy resistance [25, 26]. Exon back-splicing produces several circRNAs, which are frequently located in the cytoplasm [27]. Consistent with this, circSCP2 derived from exon 1 of SCP2 was mainly distributed in the cytoplasm and was significantly expressed in CRC tissues. Additionally, recently published research reported that IGF2BP1 acted as an adaptor protein to assist the nuclear export of circRNAs [28]. We also observed elevated exosomal circSCP2 levels in serum from patients with CRC. Accordingly, we speculated that IGF2BP1 might further help modulate the circSCP2 export pathway, thereby boosting tumor-promoting function and exosomal secretion of circSCP2. Furthermore, we explored the intracellular communication between tumor cells and CAF precursor cell LX2 via secreted exosomal circSCP2. Exosomal

circSCP2-induced activation of LX2 and normal fibroblasts can accelerate tumor growth, invasion, and metastasis [29–31]. The effects and underlying mechanisms of circRNA-loaded exosomes on tumor microenvironments have gained much attention [29, 31–34]. Moreover, our results revealed that exosomes containing circSCP2 promoted M2 macrophage polarization, and transcriptomics (Fig. 8: Visual Figure). And tumors with high expression of circSCP2 exhibit reduced sensitivity to chemotherapy,

Oxaliplatin. Taken together, this study demonstrated for the first time that high expression of plasma exosomal circSCP2 was associated with advanced stages in CRC patients. Tumor-derived circSCP2 firstly enhanced the proliferation, invasion and metastasis of tumor cells via sponging miR-92a-1-5p and interacting with PTBP1 to stabilize IGF2BP1 expression. Furthermore, tumor-secreted circSCP2-containing exosomes modulate tumor-stroma interactions including activation of

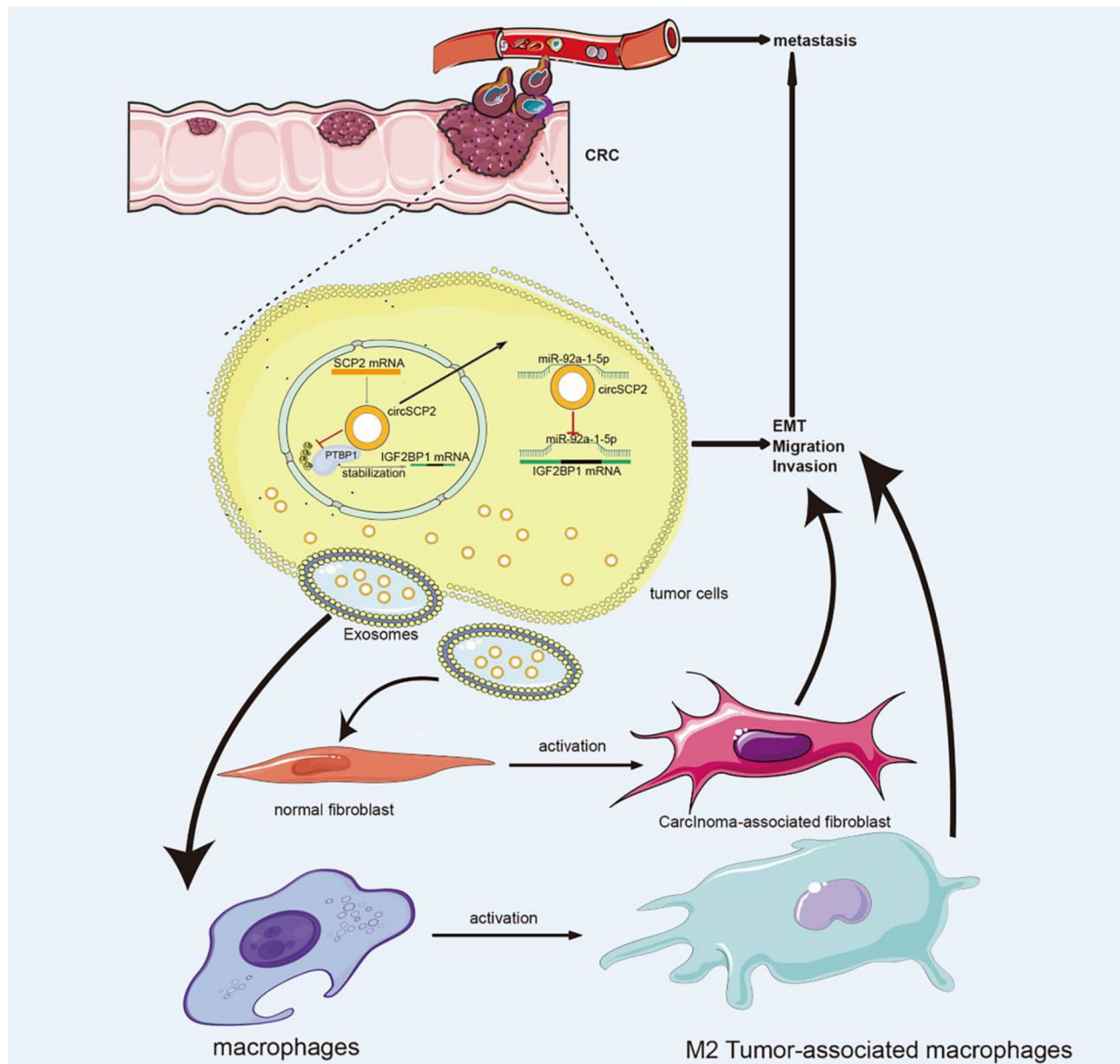


**Fig. 8** Schematic representation of the role of exosomal circSCP2 in CRC progression and metastasis. The schematic shows the effect of circSCP2 on CRC cells through sponging miR-92a-1-5p and also suppressing PTBP1 degradation, and subsequently promote EMT, tumor migration and invasion via upregulation of downstream IGF2BP1 mRNA and protein expression. Moreover, exosomal circSCP2 released by CRC tumors could either transform normal fibroblasts into activated carcinoma-associated fibroblasts, or transform macrophages into M2 tumor-associated macrophages, which further form positive feedback loops to accelerate tumor progression, invasion, migration and immunosuppression

tumor-promoting CAFs and immuno-suppressice TAMs. Our results may offer novel concepts and paradigms to suggest more attractive therapeutic approaches against circular RNAs in cancer. Further analysis is needed to provide a comprehensive profile of cancer communications and anti-cancer immunity.

#### Abbreviations

CRC	Colorectal cancer
circRNA	Circular RNAs
EXO	Exosome
IGF2BP1	Insulin-like growth factor 2 mRNA-binding protein 1
PTBP1	Polypyrimidine tract binding protein 1
RIP	RNA Immunoprecipitation
qRT-PCR	Quantitative real-time PCR
FISH	Fluorescence in situ hybridization
CCK8	Cell counting kit-8
EdU	5-ethynyl-2'-deoxyuridine
FISH	Fluorescence in situ hybridization
IHC	Immunohistochemistry
IF	Immunofluorescence
HE	Hematoxylin and eosin
CHX	Cycloheximide
CAF	Tumor-associated fibroblast
TAM	Tumor-associated macrophage

#### Supplementary Information

The online version contains supplementary material available at <https://doi.org/10.1186/s13062-024-00571-1>.

Supplementary Material 1

#### Acknowledgements

Not applicable.

#### Author contributions

Meng Qing performed in vitro and in vivo experiments and analyzed data; Meng Qing wrote the first draft of manuscript; Luo Xin participated in data analysis and critical discussion; Xiang Haoyi, Wang Yijing, Hu Kepeng, Wang Jiawei, Chen engeng, Zhang Wei and Chen Jiaxin, contributed to the study concept, research design, and finalized the manuscript. Zhangfa Song and Ju Zhenyu organized and supervised the study.

#### Funding

This study was supported by the National Natural Science Foundation of China (82273265), the Zhejiang province Research and Development Program of 'Lingyan' (No.2023C03065), the Natural Science Foundation of Zhejiang Province (LH19H160001, LY20H180014), and the Department of Health of Zhejiang Province (2018KY473, 2018PY025).

#### Data availability

No datasets were generated or analysed during the current study.

#### Declarations

##### Ethics approval and consent to participate

The animal study was approved and performed in compliance with the guidance suggestion of Animal Care Committee of Sir Run Run Shaw Hospital and carried out under the guidelines of the Guide for the Care and Use of Laboratory Animals of the China National Institutes of Health. The collection of clinical specimens was approved by the Ethics Committee of Sir Run Run Shaw Hospital after informed consent was obtained from each patient.

##### Consent for publication

Not applicable.

#### Competing interests

The authors declare no competing interests.

Received: 27 September 2024 / Accepted: 25 November 2024

Published online: 20 December 2024

#### References

- Sung H, Ferlay J, Siegel RL, Laversanne M, Soerjomataram I, Jemal A, et al. Global Cancer statistics 2020: GLOBOCAN estimates of incidence and Mortality Worldwide for 36 cancers in 185 countries. *CA Cancer J Clin*. 2021;71(3):209–49.
- Sanger HL, Klotz G, Riesner D, Gross HJ, Kleinschmidt AK. Viroids are single-stranded covalently closed circular RNA molecules existing as highly base-paired rod-like structures. *Proc Natl Acad Sci U S A*. 1976;73(11):3852–6.
- Li Z, Huang C, Bao C, Chen L, Lin M, Wang X, et al. Exon-intron circular RNAs regulate transcription in the nucleus. *Nat Struct Mol Biol*. 2015;22(3):256–64.
- Wang Y, Liu J, Ma J, Sun T, Zhou Q, Wang W, et al. Exosomal circRNAs: biogenesis, effect and application in human diseases. *Mol Cancer*. 2019;18(1):116.
- Wang R, Zhang S, Chen X, Li N, Li J, Jia R, et al. CircNT5E acts as a sponge of miR-422a to promote Glioblastoma Tumorigenesis. *Cancer Res*. 2018;78(17):4812–25.
- Qian L, Yu S, Chen Z, Meng Z, Huang S, Wang P. The emerging role of circRNAs and their clinical significance in human cancers. *Biochim Biophys Acta Rev Cancer*. 2018;1870(2):247–60.
- Du WW, Zhang C, Yang W, Yong T, Awan FM, Yang BB. Identifying and characterizing circRNA-Protein Interaction. *Theranostics*. 2017;7(17):4183–91.
- Wang Z, Li Y, Yang J, Sun Y, He Y, Wang Y, et al. CircCFL1 promotes TNBC stemness and immunoescape via deacetylation-mediated c-Myc deubiquitylation to facilitate mutant TP53 transcription. *Adv Sci (Weinh)*. 2024;11(32):e2404628.
- Pegtel DM, Gould SJ, Exosomes. *Annu Rev Biochem*. 2019;88:487–514.
- Raposo G, Stoorvogel W. Extracellular vesicles: exosomes, microvesicles, and friends. *J Cell Biol*. 2013;200(4):373–83.
- Ren GL, Zhu J, Li J, Meng XM. Noncoding RNAs in acute kidney injury. *J Cell Physiol*. 2019;234(3):2266–76.
- Wang X, Zhang H, Yang H, Bai M, Ning T, Deng T, et al. Exosome-delivered circRNA promotes glycolysis to induce chemoresistance through the mir-122-PKM2 axis in colorectal cancer. *Mol Oncol*. 2020;14(3):539–55.
- Schreiber RD, Old LJ, Smyth MJ. Cancer immunoediting: integrating immunity's roles in cancer suppression and promotion. *Science*. 2011;331:1565–70.
- Rabinovich GA, Gabrilovich D, Sotomayor EM. Immunosuppressive strategies that are mediated by tumor cells. *Annu Rev Immunol*. 2007;25:267–96.
- DeNardo DG, Ruffell B. Macrophages as regulators of tumour immunity and immunotherapy. *Nat Rev Immunol*. 2019;19:369–82.
- Bray F, Laversanne M, Sung H, Ferlay J, Siegel RL, Soerjomataram I, et al. Global cancer statistics 2022: GLOBOCAN estimates of incidence and mortality worldwide for 36 cancers in 185 countries. *CA Cancer J Clin*. 2024;74(3):229–63.
- Chen L, Shan G. CircRNA in cancer: fundamental mechanism and clinical potential. *Cancer Lett*. 2021;505:49–57.
- Ma S, Xu Y, Qin X, Tao M, Gu X, Shen L, et al. RUNX1, FUS, and ELAVL1-induced circPTN22 promote gastric cancer cell proliferation, migration, and invasion through miR-6788-5p/PAK1 axis-mediated autophagy. *Cell Mol Biol Lett*. 2024;29(1):95.
- Lin J, Lyu Z, Feng H, Xie H, Peng J, Zhang W, et al. CircPDI3/miR-449a/XBP1 feedback loop curbs pyroptosis by inhibiting palmitoylation of the GSDME-C domain to induce chemoresistance of colorectal cancer. *Drug Resist Updat*. 2024;76:101097.
- Mihailovich M, Bremang M, Spadotto V, Musiani D, Vitale E, Varano G, et al. Mir-17-92 fine-tunes MYC expression and function to ensure optimal B cell lymphoma growth. *Nat Commun*. 2015;6:8725.
- Olive V, Jiang I, He L. mir-17-92, a cluster of miRNAs in the midst of the cancer network. *Int J Biochem Cell Biol*. 2010;42(8):1348–54.
- Hou CH, Chen WL, Lin CY. Targeting nerve growth factor-mediated osteosarcoma metastasis: mechanistic insights and therapeutic opportunities using larotrectinib. *Cell Death Dis*. 2024;15(5):381.
- Yu L, Sui B, Zhang X, Liu J, Hao X, Zheng L. miR-92a-1-5p enriched prostate cancer extracellular vesicles regulate osteoclast function via MAPK1 and FoxO1. *J Exp Clin Cancer Res*. 2023;42(1):1091.

24. Rodriguez M, Bajo-Santos C, Hessvik NP, Lorenz S, Fromm B, Berge V, et al. Identification of non-invasive miRNAs biomarkers for prostate cancer by deep sequencing analysis of urinary exosomes. *Mol Cancer*. 2017;16(1):156.
25. Muller S, Glass M, Singh AK, Haase J, Bley N, Fuchs T, et al. IGF2BP1 promotes SRF-dependent transcription in cancer in a m6A- and miRNA-dependent manner. *Nucleic Acids Res*. 2019;47(1):375–90.
26. Dominissini D, Moshitch-Moshkovitz S, Schwartz S, Salmon-Divon M, Ungar L, Osenberg S, et al. Topology of the human and mouse m6A RNA methylomes revealed by m6A-seq. *Nature*. 2012;485(7397):201–6.
27. Chen LL. The expanding regulatory mechanisms and cellular functions of circular RNAs. *Nat Rev Mol Cell Biol*. 2020;21(8):475–90.
28. Ngo LH, Bert AG, Dredge BK, Williams T, Murphy V, Li W, et al. Nuclear export of circular RNA. *Nature*. 2024;627(8002):212–20.
29. Mu W, Gu P, Li H, Zhou J, Jian Y, Jia W, et al. Exposure of benzo[a]pyrene induces HCC exosome-circular RNA to activate lung fibroblasts and trigger organotropic metastasis. *Cancer Commun (Lond)*. 2024;44(7):718–38.
30. Zheng S, Hu C, Lin H, Li G, Xia R, Zhang X, et al. circCUL2 induces an inflammatory CAF phenotype in pancreatic ductal adenocarcinoma via the activation of the MyD88-dependent NF-kappaB signaling pathway. *J Exp Clin Cancer Res*. 2022;41(1):71.
31. Zhao Y, Jia Y, Wang J, Chen X, Han J, Zhen S, et al. circNOX4 activates an inflammatory fibroblast niche to promote tumor growth and metastasis in NSCLC via FAP/IL-6 axis. *Mol Cancer*. 2024;23(1):47.
32. Wang D, Wang S, Jin M, Zuo Y, Wang J, Niu Y, et al. Hypoxic exosomal circPLEKHM1-Mediated crosstalk between Tumor cells and macrophages drives Lung Cancer Metastasis. *Adv Sci (Weinh)*. 2024;11(22):e2309857.
33. Sun Z, Xu Y, Shao B, Dang P, Hu S, Sun H et al. Exosomal circPOLQ promotes macrophage M2 polarization via activating IL-10/STAT3 axis in a colorectal cancer model. *J Immunother Cancer*. 2024;12(5).
34. Deng C, Huo M, Chu H, Zhuang X, Deng G, Li W, et al. Exosome circATP8A1 induces macrophage M2 polarization by regulating the miR-1-3p/STAT6 axis to promote gastric cancer progression. *Mol Cancer*. 2024;23(1):49.

### Publisher's note

Springer Nature remains neutral with regard to jurisdictional claims in published maps and institutional affiliations.